Persistent insulating state at megabar pressures in strongly spin-orbit coupled Sr_2IrO_4

Chunhua Chen,[1,2] Yonghui Zhou,[1,*] Xuliang Chen,[1] Tao Han,[3] Chao An,[3] Ying Zhou,[3] Yifang Yuan,[1,2] Bowen Zhang,[1,2] Shuyang Wang,[1,2] Ranran Zhang,[1] Lili Zhang,[4] Changjin Zhang,[1,3,5] Zhaorong Yang,[1,3,5,†] Lance E. DeLong,[6] and Gang Cao[7,‡]

[1]*Anhui Province Key Laboratory of Condensed Matter Physics at Extreme Conditions, High Magnetic Field Laboratory, Chinese Academy of Sciences, Hefei 230031, China*

[2]*Science Island Branch of Graduate School, University of Science and Technology of China, Hefei 230026, China*

[3]*Institutes of Physical Science and Information Technology, Anhui University, Hefei 230601, China*

[4]*Shanghai Synchrotron Radiation Facility, Shanghai Advanced Research Institute, Chinese Academy of Sciences, Shanghai 201204, China*

[5]*Collaborative Innovation Center of Advanced Microstructures, Nanjing University, Nanjing 210093, China*

[6]*Department of Physics and Astronomy, University of Kentucky, Lexington, Kentucky 40506, USA*

[7]*Department of Physics, University of Colorado at Boulder, Boulder, Colorado 80309, USA*

(Received 29 January 2020; revised manuscript received 6 March 2020; accepted 20 March 2020; published 15 April 2020)

It is commonly anticipated that an insulating state will collapse in favor of an emergent metallic state at high pressures: The average electron density must increase with pressure, while the electronic bandwidth is expected to broaden and fill the insulating energy band gap. Here we report an unusually stable insulating state that persists up to at least 185 GPa in Sr_2IrO_4, the archetypical spin-orbit-driven $J_{\rm eff} = 1/2$ insulator. This study shows that the electrical resistance R of single-crystal Sr_2IrO_4 initially decreases with applied pressure P, reaches a minimum in the range 32–38 GPa, then abruptly rises to recover the insulating state with increasing P up to 185 GPa. However, evidence of a saturation of R below 80 K for $P \geqslant 124$ GPa GPa raises the possibility of a low-temperature exotic state. Our synchrotron x-ray diffraction and Raman scattering data show the emergence of the rapid increase in R is accompanied by a structural phase transition from the native tetragonal $I4_1/acd$ phase to an orthorhombic *Pbca* phase (with much reduced symmetry) at 40.6 GPa. The clear correspondence of the onset pressures of these two anomalies is key to understanding the stability of the insulating state at megabar pressures: Pressure-induced, structural distortions prevent the expected onset of metallization, despite the sizable volume compression attained at the highest pressure accessed in this study.

DOI: 10.1103/PhysRevB.101.144102

I. INTRODUCTION

It is well established that a rare interplay of on-site Coulomb repulsion, U, and strong spin-orbit interactions (SOI) has unique, intriguing consequences in 4*d* and 5*d* transition-metal oxides [1–15]. The SOI-driven $J_{\rm eff} = 1/2$ Mott insulating state in the 5*d*-transition-metal oxide Sr_2IrO_4 is a profound manifestation of this interplay [1,2]. Sr_2IrO_4 adopts a canted antiferromagnetic (AFM) state [16] with a Néel temperature $T_N = 240$ K [17–20] and an energy gap $\Delta \leqslant 0.62$ eV [21–23]. It exhibits key structural, electronic, and magnetic features similar to those of La_2CuO_4, which has inspired expectations that novel superconductivity could emerge in Sr_2IrO_4 via electron doping [9]. However, there has been no experimental confirmation of superconductivity despite intensive experimental efforts [5].

It has become increasingly clear that the conspicuous absence of superconductivity in Sr_2IrO_4 is due, in part, to structural distortions; in particular, IrO_6 octahedral rotations play a crucial role in determining the ground state [5,16,24,25]. The inherently strong SOI in Sr_2IrO_4 locks the canted Ir moments to the IrO_6 octahedra in a manner that is not seen in other materials, such as the cuprates [5,16,25,26].

Although a great deal of attention has been devoted to the possible existence of superconductivity [14], the present high-pressure study demonstrates an intriguing, relevant behavior of Sr_2IrO_4 that has thus far escaped notice: Prevous high-pressure studies [26,27] indicated that Sr_2IrO_4 does not metallize up to 55 GPa, which sharply contrasts with the conventional view that a metallic state must either emerge or persist at high pressures as the electron density increases and the electronic bandwidth broadens [28]. One of the most dramatic results that supports traditional expectations is the recently discovered superconductivity in hydrogen sulfide above 200 K at megabar pressures [29]. Moreover, a recent high-pressure study of Sr_2IrO_4 using x-ray resonant scattering reveals a suppression of long-range magnetic order by 17–20 GPa, and the possible existence of quantum paramagnetic phase at higher pressures [30]. The persistent question of a possible superconducting state for a metallic phase of Sr_2IrO_4 remains open.

Here we report electrical resistance, synchrotron x-ray diffraction (XRD), and Raman scattering data for

*Corresponding author: yhzhou@hmfl.ac.cn
†Corresponding author: zryang@issp.ac.cn
‡Corresponding author: gang.cao@colorado.edu

single-crystal Sr_2IrO_4 over a much more extended range of pressures compared to previous experiments. We find a direct correlation between a structural phase transition from the native tetragonal $I4_1/acd$ phase to a lower-symmetry orthorhombic *Pbca* phase at a critical pressure $P_c = 40.6$ GPa, and a nearly concurrent strengthening of an insulating ground state of Sr_2IrO_4 that persists up to at least 185 GPa.

Specifically, our data show the electrical resistance R of Sr_2IrO_4 initially decreases with pressure, reaching a minimum in the pressure interval, 32–38 GPa [31]. However, R then takes a remarkable turn near 38 GPa, rapidly increasing toward the value observed for the ambient insulating state. The resulting U-shaped pressure dependence of R is in qualitative agreement with earlier studies for applied pressures up to 55 GPa [26,27]. A possible onset of saturation of R emerges at $P \geqslant 124$ GPa and $T < 80$ K, which presents an intriguing deviation from the behavior below 124 GPa. In any case, the data show that an insulating state persists to 185 GPa for Sr_2IrO_4, which sharply contrasts with the known behavior of most materials. We have correlated the anomalous high-pressure behavior of R with our high-pressure XRD data that document the appearance of a pressure-induced orthorhombic *Pbca* phase. The reduction of symmetry that accompanies the orthorhombic phase is of primary significance, since it should further weaken electron hopping, and possibly underpin the peculiar avoidance of metallization by Sr_2IrO_4. These observations highlight the critical roles of lattice degrees of freedom and possible spin-orbit effects in the iridates, and shed light on the absence of superconductivity observed in doped Sr_2IrO_4 [9].

II. EXPERIMENTAL DETAILS

Sr_2IrO_4 single crystals were grown by the self-flux method described [5,17]. Given the large magnitude of resistance, a two-probe method was employed to perform the high-pressure electrical transport measurements for a temperature range of 4.5–300 K in a Be-Cu diamond anvil cell (DAC) with a rhenium gasket. We would like to emphasize that our high-pressure techniques are comparable to those employed by other groups [26,27,32–39]. Most importantly, we report on resistance measurements on single-crystal Sr_2IrO_4 for $P > 55$ GPa. Our measurements of R were conducted on single crystals of Sr_2IrO_4 in two separate runs: Run 1 and run 2 used different pressure media, and covered overlapping pressure ranges of 0.6–54 GPa and 24–185.0 GPa, respectively, which provides an assessment of the reproducibility and validity of the results [31]. For run 1, a freshly cleaved Sr_2IrO_4 single crystal was loaded with sodium chloride (NaCl) powder as the pressure transmitting medium and the electrical current was applied within the *ab* plane. This pressure transmitting medium is commonly used for pressures below 60 GPa [32]. For run 2, the same sample was squeezed between the diamond anvil and insulation layer directly without a pressure transmitting medium. This approach is also consistent with that commonly used for measurements at megabar pressures [33–36]. The culet sizes of diamond were of 300 μm and 100 μm for run 1 and run 2, respectively.

A Mao-Bell-type symmetric DAC and Daphne 7373 pressure-transmitting medium were used for the measurements of high-pressure synchrotron powder XRD and Raman scattering. A pair of diamonds with a culet of 300-μm diameter and rhenium gasket were also used for the XRD measurements. The high-pressure XRD ($\lambda = 0.6199$ Å) measurements were performed at room temperature using the beamline BL15U1 at the Shanghai Synchrotron Radiation Facility. The DIOPTAS program [40] was employed for image integrations. The Le Bail method was used to fit the XRD patterns via the RIETICA program [41]. The Raman measurements were performed at room temperature on a freshly cleaved Sr_2IrO_4 single crystal using 633-nm He-Ne laser for excitation with the power below 10 mW to avoid sample damage and any heating effect. Pressure at room temperature was calibrated by the ruby fluorescence scale below 80 GPa [42] and the diamond Raman scale above 80 GPa [43], respectively.

A more detailed description of our experimental methods is given in the Supplemental Material [31].

III. RESULTS AND DISCUSSION

We first focus on the basal-plane resistance R from the run-1 data in Fig. 1(a1) for 0.6–32.1 GPa, and Fig. 1(a2) for 37.4–54.2 GPa. R increases monotonically with decreasing temperature for $P = 0.6$ GPa, consistent with the known behavior at ambient pressure [5]. With increasing P up to 32.1 GPa, R decreases by more than two orders of magnitude at low temperatures, but retains insulating behavior [Fig. 1(a1)]. This trend reverses for $P > 32$ GPa, as shown in Fig. 1(a2): R rapidly rises and almost fully recovers its initial, ambient-pressure value. A corresponding T-P contour plot in Fig. 1(b) illustrates a U-shaped pressure dependence of R with a minimum near 32 GPa, consistent with previous results [26,27].

Data from run 2 overlap those of run 1 over a significant pressure range, 24–54 GPa; but run 2 spans a wider, much higher pressure range of 24 to 185.0 GPa [see Figs. 1(c)–1(d)]. The run-2 data confirm the results obtained in run 1, although the lowest R occurs near 38 GPa for run 2, which is somewhat higher than 32 GPa observed in run 1. (Given the inherent imperfections of high-pressure measurements, this difference is acceptable.) It is emphasized that this rapid rise of R near 38 GPa is followed/accompanied by a structural phase transition at 40 GPa. Nearly simultaneous changes in R and the crystal structure reveal a direct correlation between the retention of an insulating state and the structural distortions.

However, below 80 K and at $P \geqslant 124$ GPa, R decreases by more than 67%, compared to R at 81 GPa, and exhibits an apparent approach to saturation [Fig. 1(e)]. The tendancy toward saturation is both significant and intriguing (note the finite variation of R in the saturating regime shows that the sample retains enough integrity to respond to changes in applied pressure). Indeed, our data may indicate a possible topological insulating state, in which a saturated resistance at low temperatures could be a result of a pressure-induced surface state [44,45]. This result is interestingly relevant to a recent high-pressure study in which a possible quantum paramagnetism or a topological state in compressed Sr_2IrO_4 is suggested [30]. It is nevertheless clear that the electronic structure of Sr_2IrO_4 undergoes a significant change in the megabar range.

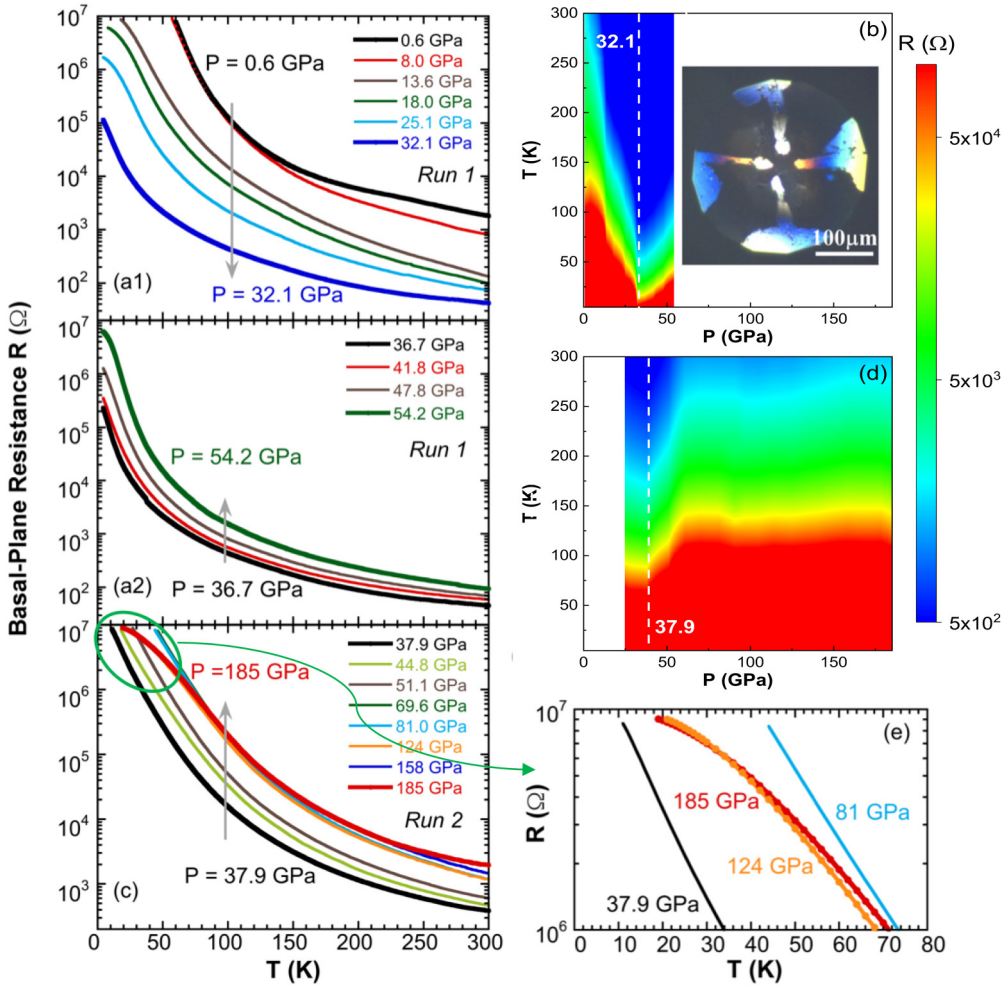

FIG. 1. The temperature dependence of the basal-plane resistance R over pressures ranging from (a1) 0.6–32.1 GPa and (a2) 36.7–54.2 GPa for run 1, and (c) 24.7–185 GPa for run 2. Note the gray arrows that indicate the increase or decrease in R with increasing P. Corresponding contour plots are shown in (b) for the pressure range 0.6–54.2 GPa for run 1 and in (d) for the pressure range 24.7–185 GPa for run 2. The colors red and blue represent the highest and lowest resistance R, respectively, and other colors indicate intermediate resistance values. The white dashed lines mark the pressure regime of 32.1−37.9 where R reaches its minimum. (e) Data marked by the green oval circle in (c) is shown in an expanded plot of the near-saturated regime for R (i.e., $P \approx 185$ GPa and $T < 80$ K). Inset: A snapshot of the diamond anvil cell with a sample at 27 GPa.

Our demonstration that the insulating state of Sr_2IrO_4 is retained to megabar pressures is extraordinary, and demands careful examination of structural properties using both XRD and Raman scattering experiments that can access pressures up to 74 GPa and 65.6 GPa, respectively. Results of our *in situ* synchrotron XRD measurements at 300 K under pressure are shown in Fig. 2(a). At $P < 40.6$ GPa, Sr_2IrO_4 retains the same structure as that at ambient pressure; i.e., the tetragonal space group $I4_1/acd$. As expected, all peaks progressively shift to higher angles, reflecting the shrinkage of the unit cell as P increases. The structural phase transition to a lower-symmetry phase is detected at a critical pressure $P_c = 40.6$ GPa: The (112) peak intensity begins to become asymmetric at 40.6 GPa, and then gradually splits into two peaks upon further compression, signaling the occurrence of a structural transition [Fig. 2(b)]. This conclusion is corroborated by the splitting of both (116) and (220) peaks, as well as the emergence of a new peak on the right shoulder of the (004) peak as the pressure reaches 51 GPa [Figs. 2(c)–2(d)]. These emergent peaks become more pronounced with increasing P and are well-indexed by an orthorhombic structure with space group *Pbca*, as shown in Fig. 3. We note this lower-symmetry structure requires both a rotation and tilt of the IrO_6 octahedra of Sr_2IrO_4 [31].

It is important to note the crystal structure of the sample recovers its ambient tetragonal phase when the pressure is reduced from 73.7 GPa to 0.1 GPa [see the green arrow in Fig. 2(a)]. This confirms the observed pressure-driven structural transition at 40.6 GPa is intrinsic. Indeed, the volume data are fitted well by the third-order Birch-Murnaghan equation of state [46], which yields the ambient pressure volume $V_0 = 97.2(0.3)$, bulk modulus $B_0 = 218.2(10.4)$, and its first-order derivative $B_0' = 3.1(0.3)$ for the low-pressure tetragonal phase (see Fig. 3(c)). Data for the high-pressure *Pbca* phase yield values $V_0 = 81.3(0.6)$ Å^3, $B_0 = 340.0(17.2)$ GPa, and $B_0' = 13.1(0.2)$ (see Fig. 3(c)). The standard Le Bail method was used for the structural refinement (see Ref. [31] for more details). We note that a pressure-induced phase transition in

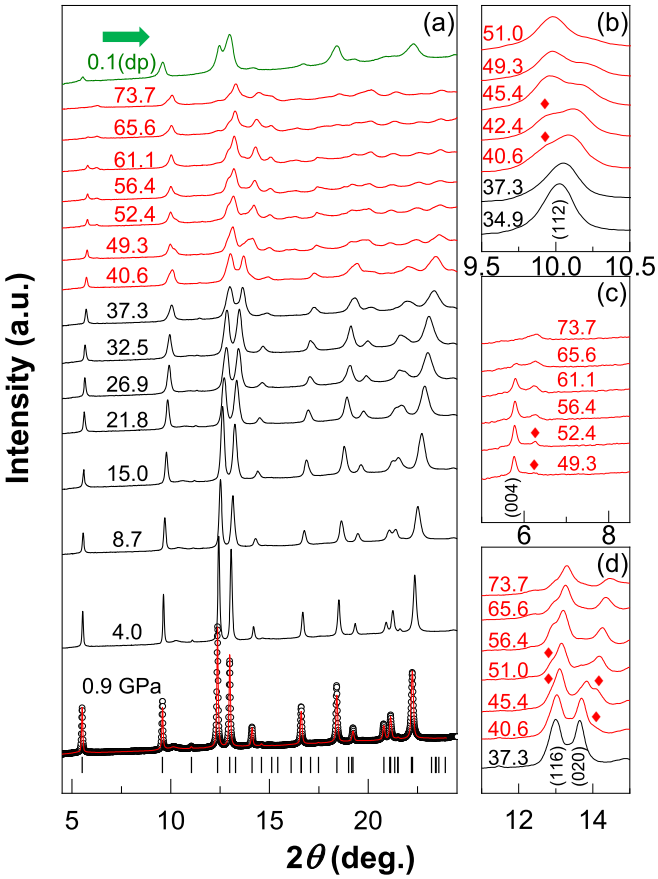

FIG. 2. (a) Representative synchrotron x-ray diffraction patterns at room temperature spanning $P = 0.9$ to 73.7 GPa. The black curves represent the native $I4_1/acd$ phase ($Z = 8$), red patterns the pressure-induced *Pbca* phase ($Z = 4$). Note that the green XRD spectrum in the top of (a) marked by a green arrow indicates that the crystal structure of the sample recovers its ambient structure after decompression (marked dp). (b)–(d) The structural transition at 40.6 GPa is marked by red rhombi. The refinement results for 0.9 GPa are shown in (a). The experimental data are the solid circles, and the calculated data are red lines. Bragg peaks are represented by black vertical sticks.

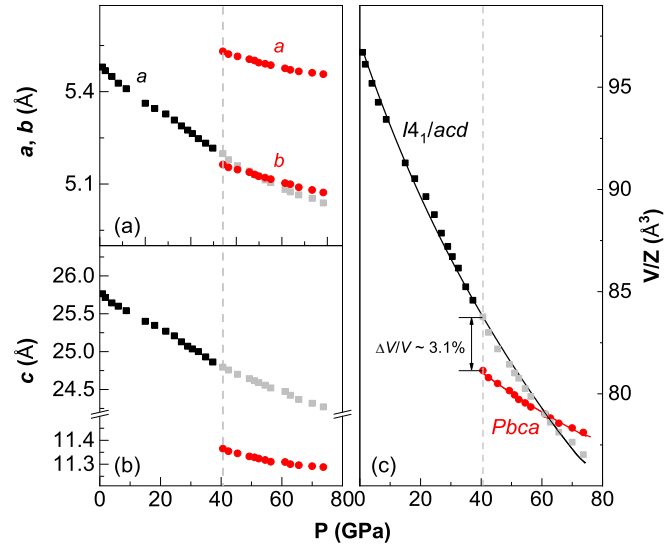

FIG. 3. Pressure dependence of the lattice parameters of (a) the a axis and b axis, (b) the c axis, and (c) the unit cell volume. The black squares and red circles represent the lattice parameters of the native $I4_1/acd$ phase ($Z = 8$) and the pressure-induced *Pbca* phase ($Z = 4$), respectively. Note that the gray dashed lines mark the critical pressure $P_c = 40.6$ GPa. For comparison and contrast, the lattice parameters for the native phase marked by the faint gray squares are plotted above P_c. The black and red solid lines represent the fits for the phases with the Birch-Murnaghan equation of states.

Sr_2IrO_4 was reported in an early study, but broad, overlapping XRD peaks observed at high pressures prevented a further refinement of the pressure-induced space group and subtle changes in octahedral tilt [47].

Raman scattering is an alternative, powerful tool for detecting small or local lattice distortions, as well as structural transitions. We conducted Raman scattering experiments at 300 K and pressures up to 65.6 GPa for comparison with the XRD data (Fig. 3). Figure 4(a) shows the selective Raman spectra at various pressures up to 65.6 GPa. At 1.0 GPa, there are four phonon peaks marked by M_1 (the merging of A_{1g} and B_{2g} modes), $M_2(A_{1g})$, $M_3(B_{2g})$, and $M_4(A_{1g})$, which are located at 177, 252, 388, and 561 cm^{-1}, respectively, in agreement with a previous report [47]. The mode M_1 represents a rotation of the IrO_6 octahedra about the c axis, combined with a Sr displacement along the $c$axis, while M_2 denotes a pure rotation of the IrO_6 octahedra about the $c$axis. Mode M_3 is an in-plane bending of the IrO_6 octahedra, and

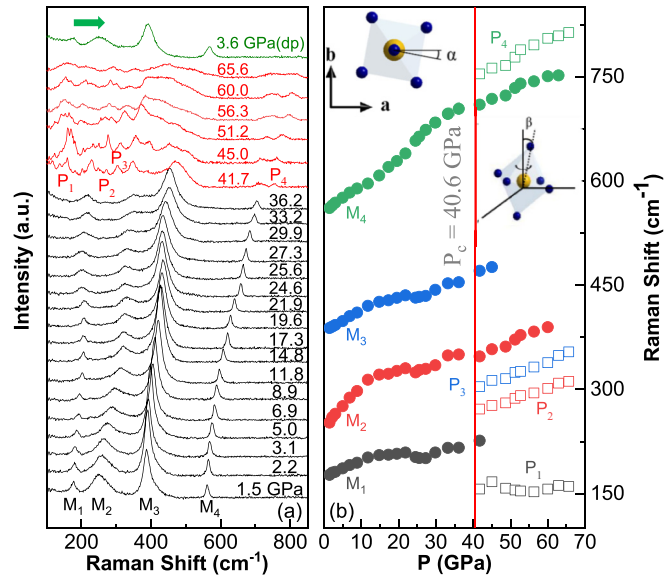

FIG. 4. (a) Selected room-temperature Raman spectra of Sr_2IrO_4 for applied pressures extending from 1.5 to 65.6 GPa. The black patterns include $M_{1\text{-}4}$; the red curves cover a series of new peaks marked $P_{1\text{-}4}$ after the structural transition. The uppermost green line is the spectrum after decompression. (b) Raman frequencies as a function of pressure for phonon modes. Note that the red solid line marks the critical pressure of 40.6 GPa, consistent with that obtained in the XRD measurements. Insets: The rotation of IrO_6 below P_c and the rotation and tilt of IrO_6 above P_c. Note that the spectrum marked by a green arrow in (a) recovers its low-pressure form after decompression back to 3.6 GPa, suggesting that the sample integrity is preserved at 65.6 GPa.

M_4 is a stretching mode involving a modulation of the Ir-O (apical) distance. With increasing P, the Raman shift of all four modes first increases linearly, then shows clear slope changes near 15 GPa; this is particularly true for the M_2 mode that measures the octahedral rotation. Moreover, the M_1, M_2, and M_3 modes display distinctly abnormal red-shifts above 22.9 GPa, which gradually evolve into a blueshift upon further compression; this behavior is consistent with a second-order phase transition: Indeed, for $P \geqslant P_c = 40.6$ GPa, a series of new peaks labeled by P_{1-4} appear, and can be attributed to the structural transition detected in the XRD measurements. It is important to note the Raman spectrum [marked by a green arrow in Fig. 4(a)] recovers its low-pressure behavior after decompression back to 3.6 GPa, which confirms the intrinsic sample behavior for pressures up to 65.6 GPa.

Both the XRD and Raman scattering data provide a direct, crucial correlation of the lattice dynamics with the transport properties at high pressures, and demonstrate that the persistent insulating state at megabar pressures is related to the significant reduction in symmetry incurred in the transition from the $I4_1/acd$ phase (32 symmetry group elements) to the lower-symmetry $Pbca$ phase (eight symmetry group elements). This structural change involves not only rotations, but also titling of IrO_6 octahedra at $P \geqslant P_c$. The striking stability of the insulating state over such a broad pressure interval of 38 to 185 GPa suggests two competing forces are at work: (1) There is a tendency for band broadening that must accompany a sizable volume compression and favors metallic behavior. (2) There is a pressure-induced crystal distortion that generally weakens electron hopping and can lead to localization, which eventually prevails in the present case, given the recovered insulating state for $P > 38$ GPa.

Nevertheless, Sr_2IrO_4 appears to defy conventional Mott physics in that the insulating state and long-range AFM order do not always precisely accompany each other [5]. An early study indicates weak ferromagnetism vanishes near 18 GPa [26], which is in the vicinity of 15 GPa, where our Raman data clearly indicate a change in the IrO_6 rotation. The weak ferromagnetism is due to magnetic canting [16], which closely tracks the IrO_6 rotation [16,25]. It is recognized that an elongation (compression) of the $c$axis weakens (enhances) the magnetic canting, or the weak ferromagnetism, and facilitates either a collinear AFM or a paramagnetic state [24]. Our XRD data show that the lattice c/a ratio increases significantly with rising pressure in both the tetragonal phase below $P_c(=40.6)$ and the orthorhombic phase above P_c (see Fig. 5). These observations offer a reasonable explanation of the disappearance of weak ferromagnetism above 18 GPa, as reported previously [26], since the enhanced c/a ratio suggests that Sr_2IrO_4 becomes more two-dimensional, which is generally unfavorable for long-range magnetic order. Our data also bear upon recent results [30] that suggest that a possible paramagnetic state exists above 18 GPa [30,48].

IV. CONCLUSION

In conclusion, our extended high-pressure study clearly documents a rare, persistent insulating state at megabar pressures and its close correlation with a pressure-induced structural phase transition in Sr_2IrO_4. We present strong evidence

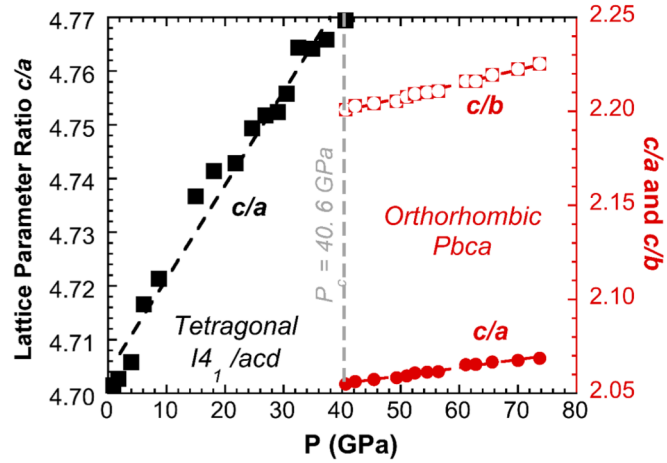

FIG. 5. The pressure dependence of the lattice parameter ratio of the c axis to the a *axis*,c/a, for the tetragonal phase (blue), and c/a and c/b for the orthorhombic phase (red).

for the unique, crucial role the lattice symmetry and dynamics play in determining ground states in spin-orbit-coupled materials. These results offer a perspective for understanding the discrepancies between recent theoretical proposals and experimental results in iridates, including the absence of superconductivity in Sr_2IrO_4.

More generally, a persistent insulating state at megabar pressures raises an intriguing, fundamental issue: The strong exchange-correlation effects supported by a high, narrow peak in the density of states near the Fermi level may not lead to traditional (metallic/delocalized) Fermi liquid screening interactions in Sr_2IrO_4, as anticipated from Mott physics. We speculate that very large volume reductions and strong Coulomb correlations alternatively can stabilize highly directional bonds. This contrasts with Hartree-Fock mean-field theories that treat breaking of spherical symmetry by electron-electron interactions via spherical averaging of self-consistent Coulomb fields. Our observation of persistent insulating behavior in Sr_2IrO_4 indicates that the Hartree-Fock methodology is not well-suited for treating situations where strong SOI and anisotropic correlations dictate that electron localization is dominant at very high densities.

ACKNOWLEDGMENTS

We are grateful for the financial support from the National Key Research and Development Program of China (Grants No. 2018YFA0305700 and No. 2016YFA0401804), the National Natural Science Foundation of China (NSFC) (Grants No. 11574323, No. U1632275, No. 11874362, No. 11804344, No. U1832209, and No. 11704387), the Users with Excellence Project of Hefei Science Center CAS (Grant No. 2018HSCUE012) and the Major Program of Development Foundation of Hefei Center for Physical Science and Technology (Grant No. 2018ZYFX002). Y.Z. was supported by the Youth Innovation Promotion Association CAS (Grant No. 2020443). The x-ray diffraction experiment was performed at the beamline BL15U1, Shanghai Synchrotron Radiation Facility (SSRF). G.C. acknowledges support from the US National Science Foundation via Grants No. DMR 1712101 and

No. 1903888. G.C. is thankful to Dr. Feng Ye, Dr. Bing Hu, and Mr. Hengdi Zhao for useful discussions. LED research is supported by U.S. National Science Foundation Grant No. DMR-1506979.

[1] B. J. Kim, H. Jin, S. J. Moon, J. Y. Kim, B. G. Park, C. S. Leem, J. Yu, T. W. Noh, C. Kim, S. J. Oh, J. H. Park, V. Durairaj, G. Cao, and E. Rotenberg, Novel $J(\mathrm{eff}) = 1/2$ Mott State Induced by Relativistic Spin-Orbit Coupling in Sr_2IrO_4, Phys. Rev. Lett. **101**, 076402 (2008).

[2] B. J. Kim, H. Ohsumi, T. Komesu, S. Sakai, T. Morita, H. Takagi, and T. Arima, Phase-sensitive observation of a spin-orbital Mott state in Sr_2IrO_4, Science **323**, 1329 (2009).

[3] W. Witczak-Krempa, G. Chen, Y. B. Kim, and L. Balents, Correlated quantum phenomena in the strong spin-orbit regime, Annu. Rev. Condens. Matter Phys. **5**, 57 (2014).

[4] J. G. Rau, E. K. H. Lee, and H. Y. Kee, Spin-orbit physics giving rise to novel phases in correlated systems: Iridates and related materials, Annu. Rev. Condens. Matter Phys. **7**, 195 (2016).

[5] G. Cao and P. Schlottmann, The challenge of spin-orbit-tuned ground states in iridates: A key issues review, Rep. Prog. Phys. **81**, 042502 (2018).

[6] R. Schaffer, E. K. H. Lee, B. J. Yang, and Y. B. Kim, Recent progress on correlated electron systems with strong spin-orbit coupling, Rep. Prog. Phys. **79**, 094504 (2016).

[7] C. Martins, M. Aichhorn, and S. Biermann, Coulomb correlations in 4d and 5d oxides from first principles-or how spin-orbit materials choose their effective orbital degeneracies, J. Phys. Condens. Matter **29**, 263001 (2017).

[8] G. M. Luke, Y. Fudamoto, K. M. Kojima, M. I. Larkin, J. Merrin, B. Nachumi, Y. J. Uemura, Y. Maeno, Z. Q. Mao, Y. Mori, H. Nakamura, and M. Sigrist, Time-reversal symmetry breaking superconductivity in Sr_2RuO_4, Nature **394**, 558 (1998).

[9] F. Wang and T. Senthil, Twisted Hubbard Model for Sr_2IrO_4: Magnetism and Possible High Temperature Superconductivity, Phys. Rev. Lett. **106**, 136402 (2011).

[10] Y. K. Kim, N. H. Sung, J. D. Denlinger, and B. J. Kim, Observation of a d-wave gap in electron-doped Sr_2IrO_4, Nat. Phys. **12**, 37 (2016).

[11] S. A. Grigera, R. S. Perry, A. J. Schofield, M. Chiao, S. R. Julian, G. G. Lonzarich, S. I. Ikeda, Y. Maeno, A. J. Millis, and A. P. Mackenzie, Magnetic field-tuned quantum criticality in the metallic ruthenate $Sr_3Ru_2O_7$, Science **294**, 329 (2001).

[12] L. Zhao, D. H. Torchinsky, H. Chu, V. Ivanov, R. Lifshitz, R. Flint, T. Qi, G. Cao, and D. Hsieh, Evidence of an odd-parity hidden order in a spin-orbit coupled correlated iridate, Nat. Phys. **12**, 32 (2016).

[13] R. A. Borzi, S. A. Grigera, J. Farrell, R. S. Perry, S. J. S. Lister, S. L. Lee, D. A. Tennant, Y. Maeno, and A. P. Mackenzie, Formation of a nematic fluid at high fields in $Sr_3Ru_2O_7$, Science **315**, 214 (2007).

[14] Y. K. Kim, O. Krupin, J. D. Denlinger, A. Bostwick, E. Rotenberg, Q. Zhao, J. F. Mitchell, J. W. Allen, and B. J. Kim, Fermi arcs in a doped pseudospin-1/2 Heisenberg antiferromagnet, Science **345**, 187 (2014).

[15] G. Cao and L. DeLong, *Frontiers of 4d- and 5d- Transition Metal Oxides* (World Scientific, London 2013).

[16] F. Ye, S. X. Chi, B. C. Chakoumakos, J. A. Fernandez-Baca, T. F. Qi, and G. Cao, Magnetic and crystal structures of Sr_2IrO_4: A neutron diffraction study, Phys. Rev. B **87**, 140406(R) (2013).

[17] G. Cao, J. Bolivar, S. McCall, J. E. Crow, and R. P. Guertin, Weak ferromagnetism, metal-to-nonmetal transition, and negative differential resistivity in single-crystal Sr_2IrO_4, Phys. Rev. B **57**, R11039 (1998).

[18] Q. Huang, J. L. Soubeyroux, O. Chmaissem, I. Natalisora, A. Santoro, R. J. Cava, J. J. Krajewski, and W. F. Peck, Neutron powder diffraction study of the crystal-structures of Sr2RuO4 and Sr_2IrO_4 at room-temperature and at 10-K, J. Solid State Chem. **112**, 355 (1994).

[19] R. J. Cava, B. Batlogg, K. Kiyono, H. Takagi, J. J. Krajewski, W. F. Peck, L. W. Rupp, and C. H. Chen, Localized-to-itinerant electron transition in $Sr_2Ir_{1-x}Ru_xO_4$, Phys. Rev. B **49**, 11890 (1994).

[20] M. K. Crawford, M. A. Subramanian, R. L. Harlow, J. A. Fernandezbaca, Z. R. Wang, and D. C. Johnston, Structural and magnetic studies of Sr_2IrO_4, Phys. Rev. B **49**, 9198 (1994).

[21] Q. Wang, Y. Cao, J. A. Waugh, S. R. Park, T. F. Qi, O. B. Korneta, G. Cao, and D. S. Dessau, Dimensionality-controlled Mott transition and correlation effects in single-layer and bilayer perovskite iridates, Phys. Rev. B **87**, 245109 (2013).

[22] S. Fujiyama, H. Ohsumi, T. Komesu, J. Matsuno, B. J. Kim, M. Takata, T. Arima, and H. Takagi, Two-Dimensional Heisenberg Behavior of $J(\mathrm{eff}) = 1/2$ Isospins in the Paramagnetic State of the Spin-Orbital Mott Insulator Sr_2IrO_4, Phys. Rev. Lett. **108**, 247212 (2012).

[23] J. X. Dai, E. Calleja, G. Cao, and K. McElroy, Local density of states study of a spin-orbit-coupling induced Mott insulator Sr_2IrO_4, Phys. Rev. B **90**, 041102 (2014).

[24] G. Jackeli and G. Khaliullin, Mott Insulators in the Strong Spin-Orbit Coupling Limit: From Heisenberg to a Quantum Compass and Kitaev Models, Phys. Rev. Lett. **102**, 017205 (2009).

[25] D. H. Torchinsky, H. Chu, L. Zhao, N. B. Perkins, Y. Sizyuk, T. Qi, G. Cao, and D. Hsieh, Structural Distortion-Induced Magnetoelastic Locking in Sr_2IrO_4 Revealed Through Nonlinear Optical Harmonic Generation, Phys. Rev. Lett. **114**, 096404 (2015).

[26] D. Haskel, G. Fabbris, M. Zhernenkov, P. P. Kong, C. Q. Jin, G. Cao, and M. van Veenendaal, Pressure Tuning of the Spin-Orbit Coupled Ground State in Sr_2IrO_4, Phys. Rev. Lett. **109**, 027204 (2012).

[27] D. A. Zocco, J. J. Hamlin, B. D. White, B. J. Kim, J. R. Jeffries, S. T. Weir, Y. K. Vohra, J. W. Allen, and M. B. Maple, Persistent non-metallic behavior in Sr_2IrO_4 and $Sr_3Ir_2O_7$ at high pressures, J. Phys. Condens. Matter **26**, 255603 (2014).

[28] Ho-Kwang Mao, Xiao-Jia Chen, Yang Ding, Bing Li, and Lin Wang, Solids, liquids, and gases under high pressure, Rev. Mod. Phys. **90**, 015007 (2018).

[29] A. P. Drozdov, M. I. Ermets, I. A. Troyan, V. Ksenofontov, and S. I. Shylin, Conventional superconductivity at 203 Kelvin

at high pressures in the sulfur hydride system, Nature **525**, 73 (2015).

[30] D. Haskel, G. Fabbris, J. H. Kim, L. S. I. Veiga, J. R. L. Mardegan, C. A. Escanhoela, Jr., S. Chikara, V. Struzhkin, T. Senthil, B. J. Kim, G. Cao, and J. W. Kim, Possible Quantum Paramagnetism in Compressed Sr_2IrO_4, Phys. Rev. Lett. **124**, 067201 (2020).

[31] See Supplemental Material at http://link.aps.org/supplemental/10.1103/PhysRevB.101.144102 for experimental details.

[32] Defen Kang, Yazhou Zhou, Wei Yi, Chongli Yang, Jing Guo, Youguo Shi, Shan Zhang, Zhe Wang, Chao Zhang, Sheng Jiang, Aiguo Li, Ke Yang, Qi Wu, Guangming Zhang, Liling Sun, and Zhongxian Zhao, Superconductivity emerging from a suppressed large magnetoresistant state in tungsten ditelluride, Nat. Commun. **6**, 7804 (2015).

[33] A. P. Drozdov, P. P. Kong, V. S. Minkov, S. P. Besedin, M. A. Kuzovnikov, S. Mozaffari, L. Balicas, F. F. Balakirev, D. e. Graf, V. B. Prakapenka, E. Greenberg, D. A. Knyazev, M. Tkacz, and M. I. Eremets, Superconductivity at 250 K in lanthanum hydride under high pressures, Nature **569**, 528 (2019).

[34] Maddury Somayazulu, Muhtar Ahart, Ajay K. Mishra, Zachary M. Geballe, Maria Baldini, Yue Meng, Viktor V. Struzhkin, and Russell J. Hemley, Evidence for Superconductivity Above 260 K in Lanthanum Superhydride at Megabar Pressures, Phys. Rev. Lett. **122**, 027001 (2019).

[35] Zhenhua Chi, Xuliang Chen, Fei Yen, Feng Peng, Yonghui Zhou, Jinlong Zhu, Yijin Zhang, Xiaodi Liu, Chuanlong Lin, Shengqi Chu, Yanchun Li, Jinggeng Zhao, Tomoko Kagayama, Yanming Ma, and Zhaorong Yang, Superconductivity in Pristine 2Ha-MoS_2 at Ultrahigh Pressures, Phys. Rev. Lett. **120**, 037002 (2018).

[36] T. Matsuoka, M. Sakata, Y. Nakamoto, K. Takahama, K. Ichimaru, K. Mukai, K. Ohta, N. Hirao, Y. Ohishi, and K. Shimizu, Pressure-induced reentrant metallic phase in lithium, Phys. Rev. B **89**, 144103 (2014).

[37] Zhen-Hua Chi, Xiao-Miao Zhao, Haidong Zhang, Alexander F. Goncharov, Sergey S. Lobanov, Tomoko Kagayama, Masafumi Sakata, and Xiao-Jia Chen, Pressure-Induced Metallization of Molybdenum Disulfide, Phys. Rev. Lett. **113**, 036802 (2014).

[38] F. Sun, H. Zheng, Y. Liu, E. D. Sandoval, C. Xu, J. Xu, C. Q. Jin, C. J. Sun, W. G. Yang, H. K. Mao, J. F. Mitchell, A. N. Kolmogorov, and D. Haskel, Electronic and structural response to pressure in the hyperkagome-lattice $Na_3Ir_3O_8$, Phys. Rev. B **98**, 085131 (2018).

[39] C. Donnerer, Z. Feng, J. G. Vale, S. N. Andreev, I. V. Solovyev, E. C. Hunter, M. Hanfland, R. S. Perry, H. M. Rønnow, M. I. McMahon, V. V. Mazurenko, and D. F. McMorrow, Pressure dependence of the structure and electronic properties of $Sr_3Ir_2O_7$, Phys. Rev. B **93**, 174118 (2016).

[40] C. Prescher and V. B. Prakapenka, *DIOPTAS*: A program for reduction of two-dimensional X-ray diffraction data and data exploration, High Press. Res. **35**, 223 (2015).

[41] B. A. Hunter, Rietica—A visual rietveld program, International Union of Crystallography Commission on Powder Diffraction Newsletter No. 20 (1998), http://www.iucr.org/iucr-top/comm/cpd/Newsletters/no20summer1998/.

[42] H. K. Mao, J. Xu, and P. M. Bell, Calibration of the ruby pressure gauge to 800 kbar under quasi-hydrostatic conditions, J. Geophys. Res. **91**, 4673 (1986).

[43] Y. Akahama and H. Kawamura, High-pressure Raman spectroscopy of diamond anvils to 250 GPa: Method for pressure determination in the multimegabar pressure range, J. Appl. Phys. **96**, 3748 (2004).

[44] M. Z. Hasan and C. L. Kane, Colloquium: Topological insulators, Rev. Mod. Phys. **82**, 3045 (2010).

[45] Xiao-Liang Qi and Shou-Cheng Zhang, Topological insulators and superconductors, Rev. Mod. Phys. **83**, 1057 (2011).

[46] F. Birch, Finite elastic strain of cubic crystals, Phys. Rev. **71**, 809 (1947).

[47] K. Samanta, F. M. Ardito, N. M. Souza-Neto, and E. Granado, First-order structural transition and pressure-induced lattice/phonon anomalies in Sr_2IrO_4, Phys. Rev. B **98**, 094101 (2018).

[48] M. Hermele, T. Senthil, M. P. A. Fisher, P. A. Lee, N. Nagaosa, and X. G. Wen, Stability of U(1) spin liquids in two dimensions, Phys. Rev. B **70**, 214437 (2004).